

REPORT RE- 732

**DIRECTIONAL SOLIDIFICATION OF Bi-Mn ALLOYS  
USING AN APPLIED MAGNETIC FIELD**

APRIL 1987

Final Report on Contract NAS8-36106  
Reporting Period: 1 January 1984 - 31 December 1986

prepared by

J.L. DeCarlo and R.G. Pirich

Materials and Structural Mechanics  
Grumman Corporate Research Center  
Bethpage, NY 11714-3580

for

George C. Marshall Space Flight Center  
Marshall Space Flight Center, Alabama 85812

(NASA-CR-179127) DIRECTIONAL SOLIDIFICATION  
OF Bi-Mn ALLOYS USING AN APPLIED MAGNETIC  
FIELD Final Report, 1 Jan. 1984 - 31 Dec.  
1986 (Grumman Aerospace Corp.) 46 p  
Avail: NTIS HC A03/MF A01

N87-24556

Unclas  
0082251

CSSL 11F G3/26

REPORT RE- 732

**DIRECTIONAL SOLIDIFICATION OF Bi-Mn ALLOYS  
USING AN APPLIED MAGNETIC FIELD**

**APRIL 1987**

Final Report on Contract NAS8-36106  
Reporting Period: 1 January 1984 - 31 December 1986

prepared by

J.L. DeCarlo and R.G. Pirich

Materials and Structural Mechanics  
Grumman Corporate Research Center  
Bethpage, NY 11714-3580

for

George C. Marshall Space Flight Center  
Marshall Space Flight Center, Alabama 85812

Approved by:

  
Richard A. Scheuing, V.P.  
Corporate Research Center

## ABSTRACT

Off-eutectic compositions of Bi-Mn were directionally solidified in applied transverse magnetic fields up to 3 kG, to determine the effects on thermal and solutal convection. Plane front directional solidification of eutectic and near-eutectic Bi-Mn results in a two-phase rod-like morphology consisting of ferromagnetic MnBi rods in a Bi solid solution matrix. Compositions on either side of the eutectic were studied in growth orientations vertically up and down. Temperature gradient was monitored during growth by means of an in-situ thermocouple.

For Bi-rich compositions, the magnetic field appeared to increase mixing as determined from thermal, morphological, chemical, and magnetic analysis. For Mn-rich compositions, morphological and chemical analyses suggest some reduction in mixing due to application of the magnetic field. Conductivity gradients in the melt are suggested as a possible mechanism for the observed results.

The capability for carrying out directional solidification of Bi-Mn in high longitudinal magnetic fields was established. A cross-sectional polish along the growth direction of a eutectic Bi/MnBi sample, grown at a rate of 0.5 cm/h in longitudinal fields up to 40 kG, showed evidence of aligned rod growth occurring for field strengths of 16-18 kG.

PRECEDING PAGE BLANK NOT FILMED

## CONTENTS

<u>Section</u>		<u>Page</u>
1.	INTRODUCTION AND BACKGROUND.....	1
2.	EXPERIMENTAL PROCEDURES.....	5
3.	RESULTS AND DISCUSSION.....	11
3.1	Bi-rich Samples.....	14
3.1.1	Composition A (0.2 w/o Mn).....	14
3.1.2	Composition B (0.52 w/o Mn).....	19
3.2	Mn-rich Samples.....	25
3.2.1	Composition D (0.86 w/o Mn).....	25
3.2.2	Composition E (1.5 w/o Mn).....	27
3.3	High-field Eutectic Growth.....	33
4.	SUMMARY OF Bi-Mn STUDY.....	37
5.	PROGRAM ASSOCIATED PUBLICATIONS & PRESENTATIONS.....	39
6.	ACKNOWLEDGMENTS.....	41
7.	REFERENCES.....	43

PRECEDING PAGE BLANK NOT FILMED

## ILLUSTRATIONS

<u>Figure</u>		<u>Page</u>
1	Bi-rich Portion of the Bi-Mn System.....	2
2	Ampoule Design for Directional Solidification.....	6
3	Temperature Profiles Observed in Laboratory Furnace.....	7
4	Apparatus Used for Directional Solidification of Bi-Mn in Homogeneous Magnetic Field.....	9
5	Magnetic Effect Possible through Application of External Magnetic Field.....	12
6	Rayleigh Number for Bi in Bi-Mn Melt.....	13
7	Lykoudis Number for Liquid Bi Showing Effect of Increasing Applied Magnetic Field.....	15
8	Longitudinal Composition Profile for 0.2 w/o Mn Samples (with and without an Applied Transverse Magnetic Field) a) Growth Vertically Up; b) Growth Vertically Down.....	17
9a	Temperature Gradient in Samples of Composition 0.2 w/o Mn Grown Up; A1 with an Applied Transverse Magnetic Field of B = 0 kG, and A3 with B = 3 kG.....	20
9b	Temperature Gradient in Samples of Composition 0.2 w/o Mn Grown Down; A2 with an Applied Transverse Magnetic Field of B = 0 kG, and A4 with B = 3 kG.....	21
10	Comparison of Dendritic-cooperative Transition Regions of High Thermal Gradient Samples A6 and A7 Grown Up, with and without an Applied Transverse Magnetic Field. Melt Temperature was 600 °C.....	22
11	Temperature Gradient in Samples of Composition 0.52 w/o Mn Grown Vertically Up and Down with and without an Applied Transverse Magnetic Field.....	23
12	Longitudinal Composition Profiles for 0.52 w/o Mn Samples (with and without an Applied Transverse Magnetic Field) a) Growth Up; b) Growth Down.....	24
13	Longitudinal Composition Profiles for 0.52 w/o Mn Samples Showing Variation Obtained in Macroseggregation with Different Applied Magnetic Field Strengths.....	26

PRECEDING PAGE BLANK NOT FILMED

ILLUSTRATIONS (Contd)

<u>Figure</u>		<u>Page</u>
14	Temperature Gradient in samples of Composition 0.86 w/o Mn Growth Up and Down with and without an Applied Transverse Magnetic Field.....	28
15	Longitudinal Composition Profiles for 0.86 w/o Mn Samples Growth Down with and without and Applied Transverse Magnetic Field.....	29
16	Longitudinal Composition Profiles for 1.5 w/o Mn Samples Growth Up with and without an Applied Transverse Magnetic Field: a) E1; B = 0 kG, b) E3; B = 3 kG.....	32
17	Comparison of Dendrite Growth Behavior on Samples of 1.5 w/o Mn Growth Up, with and without an Applied Transverse Magnetic Field (Longitudinal Polish).....	34
18	Photomicrograph Showing Region of MnBi Rod Growth in a Eutectic Sample of Bi-Mn Grown Up at a Velocity of 0.5 cm/h in an Applied Longitudinal Magnetic Field Swept from 0 to 40 kG in 100 min.....	35

TABLES

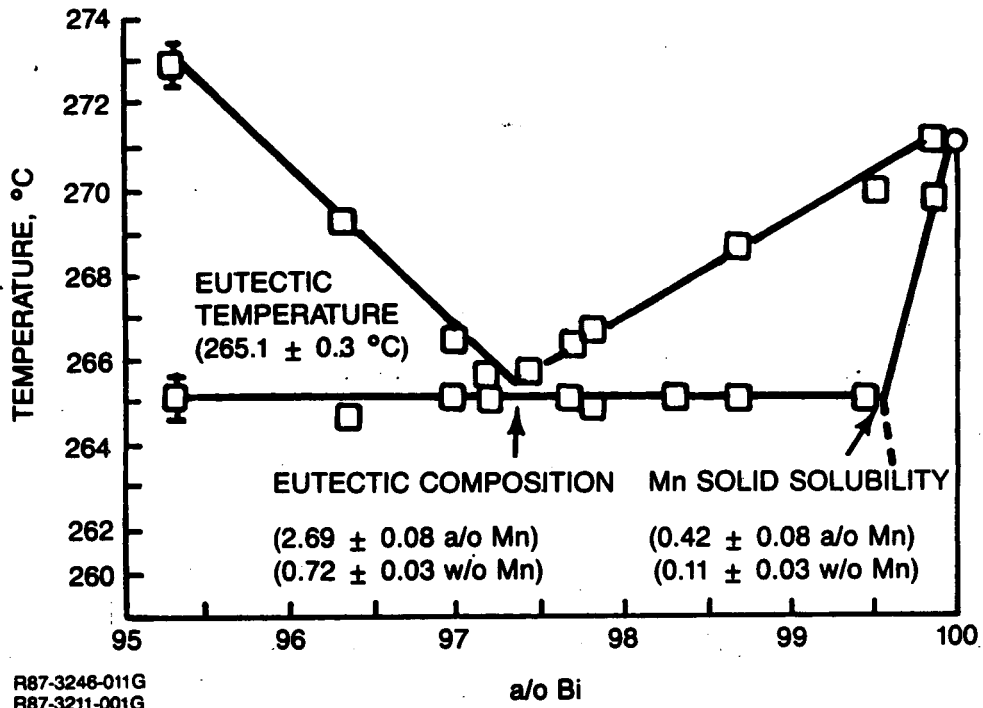
<u>Table</u>		<u>Page</u>
1	Solidification Characteristics of Bi-rich Samples.....	16
2	MnBi Mean Rod Diameters and Interrod Spacings for Selected Samples of Composition 0.52 w/o Mn.....	18
3	Solidification Characteristics of Mn-rich Samples.....	30
4	MnBi Mean Rod Diameters and Interrod Spacings for Selected Samples of Composition 0.86 w/o Mn.....	31

## 1. INTRODUCTION AND BACKGROUND

The microstructure of directionally solidified eutectic and near-eutectic Bi-Mn is characterized by two-phase growth with an aligned rod morphology, the primary phase being Bi solid solution and the secondary phase a ferromagnetic intermetallic compound of MnBi rods. Figure 1 shows the region of interest in the Bi-Mn phase diagram. Rod diameter, interrod spacing and rod alignment which are dependent on growth rate, degree of convection present in melt, and temperature gradient provide parameters to characterize the growth (Ref 1). Additionally, the equilibrium phase of MnBi exhibits strong ferromagnetism dependent on rod diameter and interrod spacing thus providing an additional parameter with which to characterize growth conditions (Ref 2 and 3).

Thermal and solutal convection can occur in the melt during vertical Bridgman crystal growth in the presence of an acceleration field, i.e., gravitational and/or spin-induced (Ref 4 and 5). Previous studies (Ref 6 to 9) have indicated that growth in a low-g environment ( $10^{-4}g_e$ ) produces a decrease in MnBi rod diameter, interrod spacing and solidification temperature, and also enhances magnetic properties. Other studies have shown that under certain growth conditions a static, uniform magnetic field can also inhibit thermal convection (Ref 10 to 12). In the first-year effort of the "Thermal and Solutal Convection Damping Using an Applied Magnetic Field" program (NAS8-34922), Bridgman-Stockbarger vertical directional solidification of eutectic Bi-Mn in transverse magnetic fields up to 3 kG resulted in samples that showed remarkable similarities to low-g growth at 30 cm/h and 50 cm/h (Ref 13 and 14). At solidification velocities below 3 cm/h, a 3 kG magnetic field had little, if any, effect on sample morphology, and the Lorentz force,  $(\bar{q} \times \bar{B})$ , would indicate that the lower growth rates in the Bi-Mn eutectic system resulted in slower convective flow. This contention is also supported by a theoretical fluid flow study by Wilcox et al (Ref 15). Solutal convection may be a significant factor in the lower growth rate region ( $V \leq 3$  cm/h) and the objectives of the present study were to:

- o Determine the effect of magnetic fields on solutal instabilities during directional solidification
- o Develop the technology and initiate studies for directional solidification in high magnetic fields ( $3 \text{ kG} \leq B \leq 40 \text{ kG}$ ).



R87-3248-011G  
R87-3211-001G

Fig. 1 Bi-rich Portion of the Bi-Mn System

For the first objective, off-eutectic compositions of Bi-Mn were directionally solidified vertically up and down (anti-parallel and parallel to the gravity vector) in transverse, static magnetic fields up to 3 kG. The melt can either be solutally stable or unstable, depending on choice of enriched species (Mn or Bi) and growth orientation (up or down). Mn has a lower fluid density than Bi and so in Bi-rich compositions, solute rejection at the interface results in enrichment of the liquid layer in front of the interface with Mn. Thus, for vertical upward solidification, the melt is solutally unstable (thermally stable). Downward solidification produces a solutally stable but thermally unstable melt. A Mn-rich composition would result in the inverse solutal stability condition since Bi is rejected at the interface (thermal stability would be identical to the Bi-rich case). In addition, previous studies (Ref 7 and 9) have shown that macrosegregation in off-eutectic Bi-Mn directional solidification follows a constitutional supercooling criterion for the Bi-rich compositions although the Mn-rich compositions show an enhanced stability region over that predicted by Mollard and Flemings (Ref 16). The condition for no constitutional supercooling was given by the latter as,

$$G_L/V = -m(C_E - C_S)/D \quad (1)$$

for two phase growth ( $C_O > kC_E$ ). Here,  $G_L$  = thermal gradient in the melt;  $V$  = growth rate;  $m$  = slope of liquidus;  $C_E$  = eutectic composition;  $C_S$  = solid composition at the interface;  $D$  = diffusivity of Mn in the melt, taken as  $2 \times 10^{-5}$  cm<sup>2</sup>/s and  $k$  = ratio of solute concentration in the melt to solute concentration in the solid at the interface. For  $C_O < kC_E$ , growth is single phase and the stability criterion would be that of Tiller et al (Ref 17):

$$G_L/V \geq mC_O(1-k/k)/D \quad (2)$$

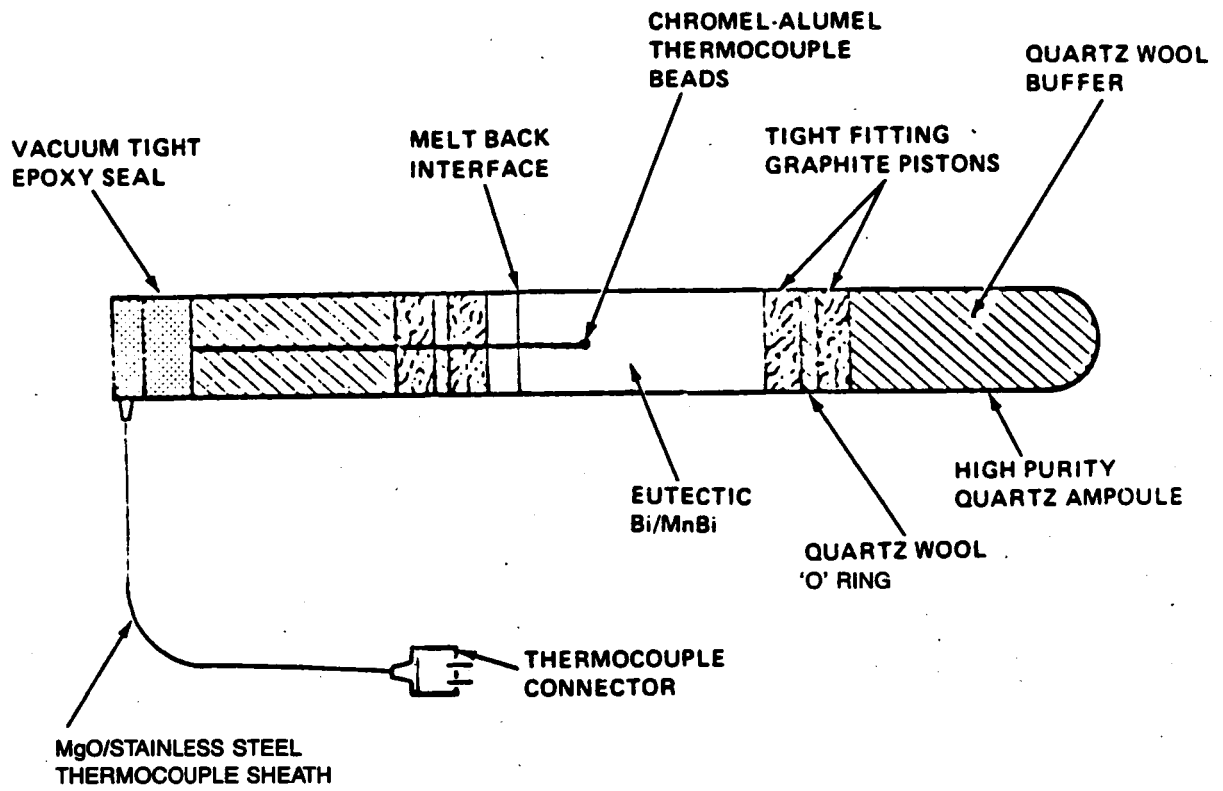
In the present study, for compositions far from the eutectic (0.2 w/o Mn and 1.5 w/o Mn) the gradient of constitutional supercooling,  $G_L/V$ , was made large ( $\geq 6 \times 10^5$  °C-s/cm<sup>2</sup>) to insure cooperative growth. For compositions closer to the eutectic (0.56 w/o Mn and 0.86 w/o Mn), the  $G_L/V$  ratio was reduced ( $\sim 3 \times 10^4$  °C-s/cm<sup>2</sup>) in an attempt to observe any effect that the magnetic field might have on constitutional supercooling.

The second objective (high field directional solidification) required modifications to the ADSF GE furnace to conform to the dimension restrictions of the bore of the 10L magnet at the Francis Bitter National Magnet Laboratory where the experiment was performed. Eutectic Bi-Mn (w/o Mn = 0.72) was directionally solidified in a vertical upward orientation at speeds of 0.5 cm/h and 1 cm/h with a field sweep rate of 400 Oe/min to a maximum field of 40 kG for each growth rate.

## 2. EXPERIMENTAL PROCEDURES

Bi-Mn alloy samples were prepared using commercially pure Mn (99.9%) and high purity Bi (99.999%) with hypoeutectic bulk compositions of  $0.2 \pm 0.06$  w/o Mn and  $0.52 \pm 0.04$  w/o Mn, and hypereutectic compositions of  $0.86 \pm 0.05$  Mn and  $1.5 \pm 0.1$  w/o Mn. The constituent elements were melted together in an evacuated ( $10^{-5}$  torr) high purity quartz crucible (1.0 cm inner diameter) above  $446^\circ\text{C}$ , the temperature at which the stoichiometric compound MnBi forms. The melt was electromagnetically stirred for 8 h to ensure homogenization. Each of these starting samples was then remelted in a specially designed, evacuated quartz crucible (0.4 cm inner diameter) and directionally solidified (see Fig. 2).

Solidification was performed both parallel (down) and anti-parallel (up) with respect to the direction of gravity. Melt temperatures were  $450^\circ\text{C}$  for the  $0.52$  w/o Mn and  $0.86$  w/o Mn samples,  $525^\circ\text{C}$  for the  $0.2$  w/o Mn and  $1.5$  w/o Mn samples. Additionally, two samples of  $0.2$  w/o Mn were set at  $600^\circ\text{C}$  in the melt to determine magnetic effects on higher thermal gradient growth. Directional solidification was performed using the Bridgman-Stockbarger method in the automatic directional solidification furnace (ADSF) apparatus built by General Electric. The furnace produced a very controlled and unidirectional thermal gradient near the adiabatic or insulating zone as shown in Fig. 3. This zone was located between a hot zone composed of nichrome heating elements and a continuously fluid-cooled copper quench block cold zone. The furnace assembly translated about the stationary quartz sample crucible. The sample crucibles were instrumented with a single in-situ, chromel-alumel thermocouple sheathed in MgO insulation and stainless steel. The thermocouple sheath was 0.025 cm with a thermal conductivity very close to that of liquid Bi. The presence of the thermocouple probe did not appear to perturb the solidification processing either through chemical contamination or heat transfer. Thermocouple temperatures were recorded using a Digital MINC-II minicomputer, and the thermal gradients were obtained from temperature vs time profiles. The field strength between the pole faces was calibrated to determine uniformity. A Hall probe with a model D855 Dyna-Empire gaussmeter was used to measure field strength vs current and voltage with and without the furnace assembly present. The furnace, consisting largely of non-magnetic material, had negligible effect on field uniformity. Any ferromagnetic parts were far enough from the pole faces not to disturb field strength or shape



R87-3246-001G  
0130-004D

Fig. 2 Ampoule Design for Directional Solidification

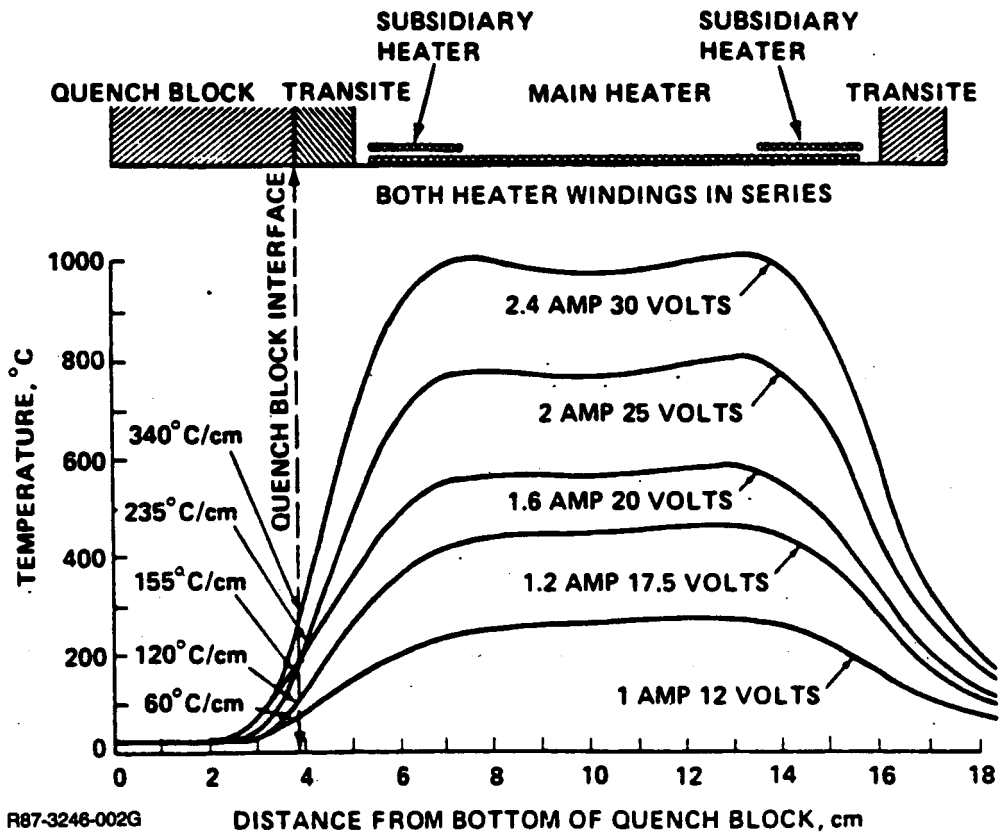


Fig.3 Temperature Profiles Observed in Laboratory Furnace

(Ref 18). Figure 4 is a photograph of the furnace/magnet apparatus used in the study.

Selected samples were metallographically examined transverse and longitudinal to the solidification direction using standard abrasive polishing techniques. Quantitative interrod and rod diameter spacings were determined on selected regions using a Leitz particle-size analysis technique. Bulk Mn concentration and MnBi volume fraction were determined on some samples using magnetic property correlations developed in previous studies (Ref 2 and 3). Magnetization measurements were carried out on small (0.4 - 0.8 gm) cylindrical samples at the Francis Bitter National Magnet Laboratory in Cambridge, Massachusetts, using a low-frequency vibrating sample magnetometer. The samples were oriented with the long rod axis (easy axis of magnetization) parallel to the field direction and subjected to fields up to 230 kG for determination of intrinsic coercivity. The transition from aligned, cooperative growth of the MnBi rods to non-aligned, cellular or dendritic structure was found to be accurately monitored by noting an abrupt decrease in both remanent magnetization and intrinsic coercivity. Mn concentration was also determined by wet chemical analysis using plasma emission spectroscopy.

Solidification of eutectic Bi-Mn in longitudinal (parallel to growth direction) magnetic fields of up to 40 kG was carried out at the Francis Bitter National Magnet Laboratory on the 10L magnet. The mounting fixture of the ADSF General Electric furnace was modified to fit within the 10-inch bore of the magnet. The furnace was positioned such that the sample, (which remains stationary while the furnace/chill block translates) was located in the center of the bore along the axis. Calibration data from the National Magnet Laboratory on the 10L magnet on field uniformity showed that the sample should be within 1% of the set field. Furnace velocity was 0.5 cm/h for the first half of the sample then 1.0 cm/h for the remainder. For each velocity the longitudinal magnetic field was swept from 0 kG to 40 kG and back to 0 kG in 200 minutes total time (linear variation). An in-situ thermocouple located 1-inch from the bottom of the Bi-Mn eutectic sample provided thermal information during the experiment which was recorded on a Digital MINC-II minicomputer.

ORIGINAL PAGE IS  
OF POOR QUALITY

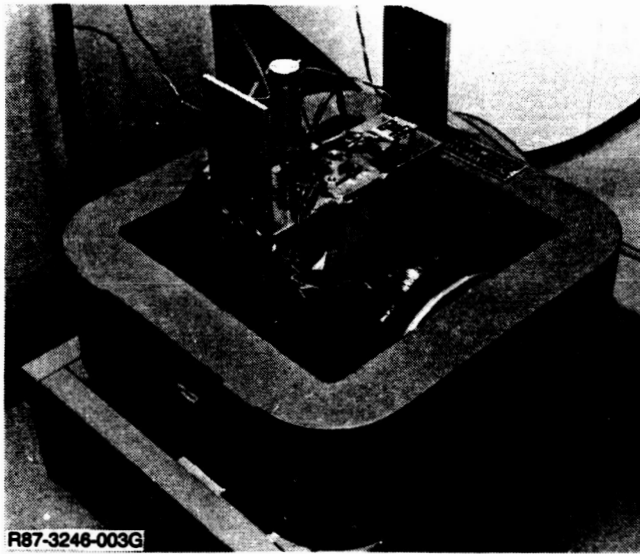


**Fig. 4 Apparatus Used for Directional Solidification  
of Bi-Mn in Homogeneous Magnetic Field**

### 3. RESULTS AND DISCUSSION

Since the components of the Bi-Mn melt are conductive, an externally imposed, constant magnetic field will interact with the fluid flow generated in the melt through the Lorentz force. The Lorentz force is proportional to the current density, where

$$\bar{j} = \sigma(\bar{E} + \bar{v} \times \bar{B}) \quad (1)$$

Here  $\sigma$  = electrical conductivity;  $\bar{E}$  = electric field = 0 for this case;  $\bar{v}$  = fluid velocity; and  $\bar{B}$  = magnetic flux. Thus the magnetic field serves to redirect the flow field via the cross-product term. Magnetic suppression of turbulent flow has been well documented (Ref 10 and 11).

It is useful to define several dimensionless quantities to characterize the melt and the interaction of the Lorentz force on the flow. The magnetic force dominates the liquid viscosity when the Hartmann number,  $M_H$ , where

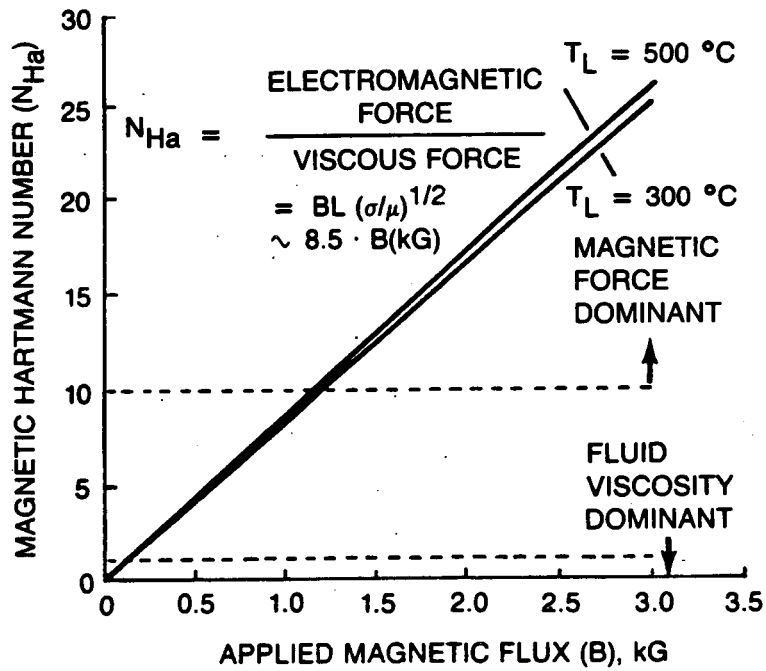
$$M_H = BL (\sigma/\mu)^{1/2} \quad (2)$$

is large compared to unity. Here  $L$  = characteristic length and  $\mu$  = viscosity. In these calculations, the characteristic length chosen was 0.4 cm corresponding to the sample diameter. A plot of the Hartmann number versus magnetic flux for Bi is given in Fig. 5 for two melt temperatures and displays a weak temperature dependence. Thus, for the field range we are operating in ( $1.6 \leq B \leq 4$  kG), the magnetic effects dominate liquid viscosity.

Another parameter of interest is the Rayleigh number,  $N_{RA}$ , which is the ratio of buoyancy force to viscous force and provides an indication of turbulence onset. It is defined as

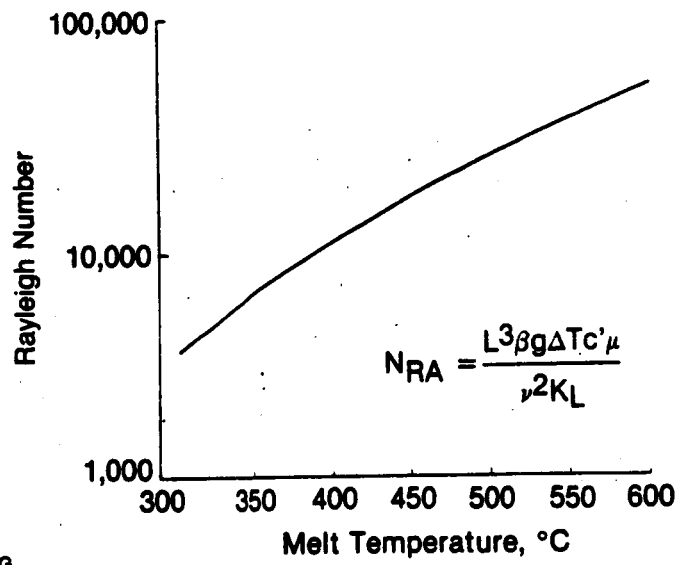
$$N_{RA} = L^3 \beta g \Delta T c' \mu / \nu^2 K_L \quad (3)$$

where  $\beta$  = coefficient of thermal expansion;  $g$  = acceleration of gravity;  $\Delta T$  = temperature differential;  $c'$  = specific heat;  $\mu$  = viscosity of melt;  $\nu$  = kinematic viscosity;  $K_L$  = thermal conductivity. Figure 6 shows the variation of  $N_{RA}$  with temperature for Bi. For  $N_{RA} \gg 1$ , convection effects dominate. Turbulence for similar but larger geometries has been shown to occur for  $N_{RA}$



R87-3246-012G  
 R87-3211-015G

**Fig. 5 Magnetic Effect Possible through Application of External Magnetic Field**



R87-3248-013G  
R87-3211-003G

Fig. 6 Rayleigh Number for Bi in Bi-Mn Melt

$\sim 10^5$  (Ref 10 and 11). In small diameter samples such as the size under study, one might then expect turbulence effects to occur for values for  $N_{RA} > 10^5$ . Figure 6 shows that Bi-Mn should have  $N_{RA}$  beneath this value for the processing conditions used. Thus, laminar flow should predominate.

Lastly, the Lykoudis number  $N_{LY}$ , provides a comparison of the magnetic body force to inertial and bouyancy forces:

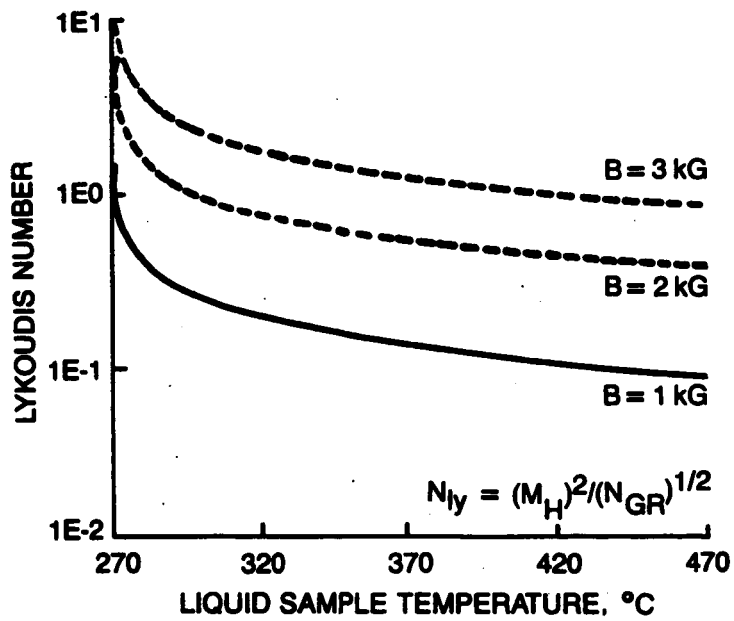
$$N_{LY} = \frac{B^2 g \left[ \frac{L}{\rho g \Delta T} \right]^{1/2}}{\left( \frac{M_H}{N_{GR}} \right)^{1/2}} \quad (4)$$

where  $N_{GR}$  = Grashof number. Here,  $\rho$  = density of liquid Bi. The Lykoudis number is plotted versus Bi temperature in Fig. 7 for several values of magnetic flux. As the melt approaches the solidification temperature, the effect of the magnetic field increases substantially (bouyancy forces are weaker). Note also that the 3 kG field exceeds unity (magnetic force stronger) at a melt temperature of around 400 °C whereas the 1 kG field barely exceeds unity even at 270 °C, very close to the solidification temperature of eutectic Bi-MnBi (265.1 °C). In a previous study of eutectic Bi-Mn (Ref 13 and 14), an applied transverse magnetic field reduced thermally driven convective fluid flow such that the resultant morphology closely resembled low-g growth. In the current study of off-eutectic Bi-Mn, the solute redistribution at the melt-solid interface will be shown to undergo a strong interaction with the transverse magnetic field.

### 3.1 BI-RICH SAMPLES

#### 3.1.1 Composition A (0.2 w/o Mn)

Table 1 shows the resulting solidification parameters for Bi-rich samples. Macrosegregation curves for composition A samples show dendritic, or cellular, structure for the first part of the growth, transitioning to cooperative growth late in the sample due to the low amounts of Mn present, shown in Fig. 8a and 8b. Although it appears that the samples grown with an imposed magnetic field of 3 kG transitioned to cooperative growth sooner than their counterparts grown at  $B = 0$  kG, the earlier transition can probably be attributed to the higher starting Mn concentration for these samples as can be seen from Table 2.



R87-3246-004G

Fig. 7 Lykoudis Number for Liquid Bi Showing Effect of Increasing Applied Magnetic Field

**Table 1 Solidification Characteristics of Bi-rich Samples**

<u>Sample</u>	<u>w/o Mn</u>	<u>Growth Rate (cm/h)</u>	<u>Growth Direction</u>	<u>Field Strength (kG)</u>	<u>G/V (<math>^{\circ}\text{C}\cdot\text{s}/\text{cm}^2</math>)</u>	<u><math>p\delta</math></u>
A1	0.119	0.73	up	0	$7.9 \times 10^5$	-
A2	0.129	0.72	down	0	$8.5 \times 10^5$	-
A3	0.224	0.82	up	3	$4.4 \times 10^5$	-
A4	0.197	0.81	down	3	$7.1 \times 10^5$	-
A6	0.26(est.)	0.7(est.)	up	3	$7.7 \times 10^5$ (est.)	-
A7	0.26(est.)	0.7(est.)	up	3	$7.7 \times 10^5$ (est.)	-
B1	0.55	10(est.)	up	0	$3.9 \times 10^4$ (est.)	2.00
B2	0.50	9.34	down	0	$4.4 \times 10^4$	2.56
B3	0.59	8.9	up	3	$3.2 \times 10^4$	0.46
B3-3	0.53	10.12	up	2.4	—	0.94
B3-2	0.49	10.54	up	1.6	—	1.23
B4	0.48	10(est.)	down	3	$2.8 \times 10^4$	0.81

R87-3211-011G  
R87-3246-021G

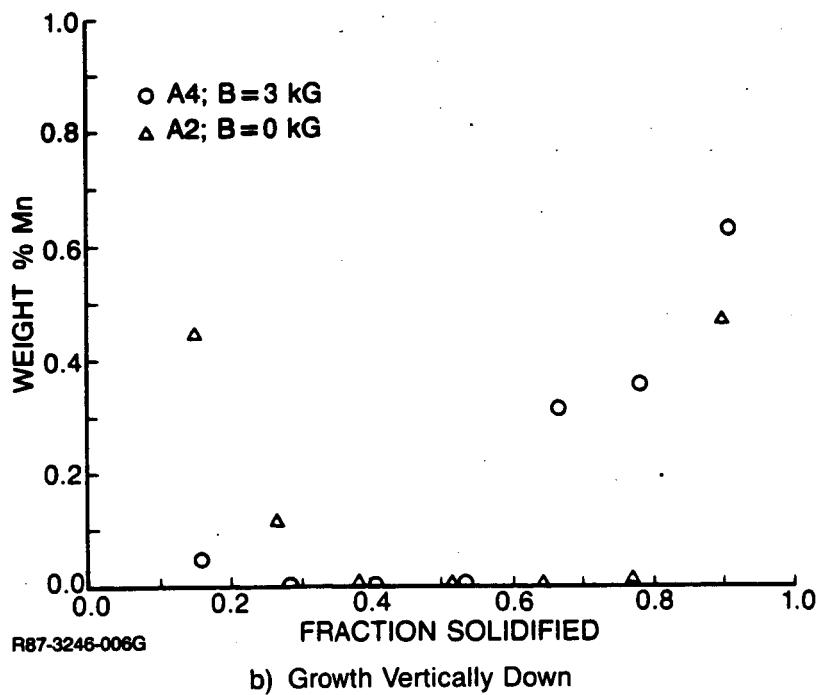
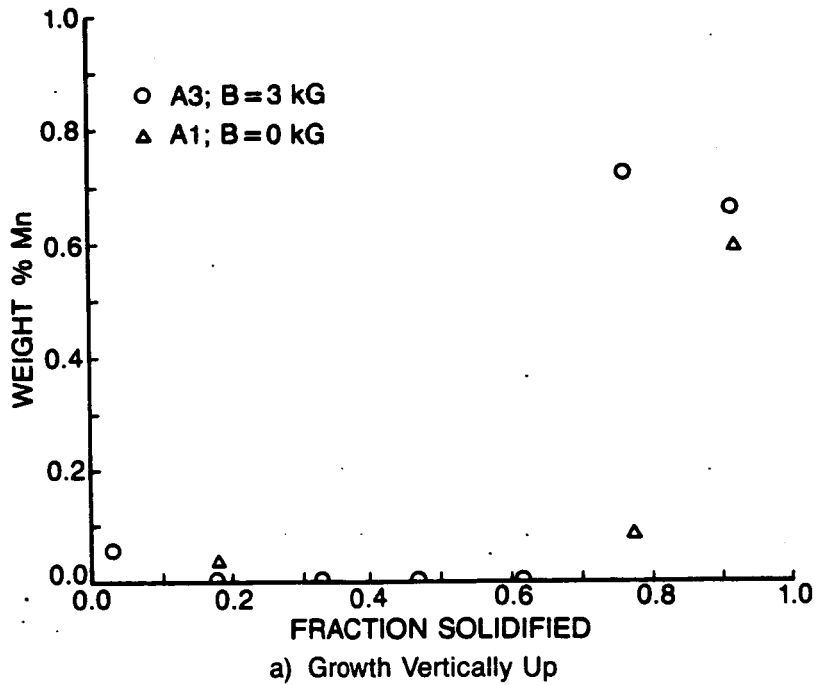


Fig. 8 Longitudinal Composition Profile for 0.2 w/o Mn Samples (with and without an Applied Transverse Magnetic Field)

**Table 2 MnBi Mean Rod Diameters and Interrod Spacings for Selected Samples of  
Composition 0.52 w/o Mn**

<u>Sample</u>	<u>B1d</u>	<u>B2d</u>	<u>B3d</u>	<u>B4d</u>
Fraction solidified, f	0.48	0.48	0.58	0.61
Mean rod diameter	$0.612 \pm 0.179$	$0.595 \pm 0.176$	$0.68 \pm 0.188$	$0.574 \pm 0.174$
Mean interrod spacing	$2.854 \pm 0.873$	$3.129 \pm 0.869$	$3.173 \pm 0.872$	$2.452 \pm 0.779$
Growth	Up, B=0 kG	Down, B=0 kG	Up, B=3 kG	Down, B=3 kG

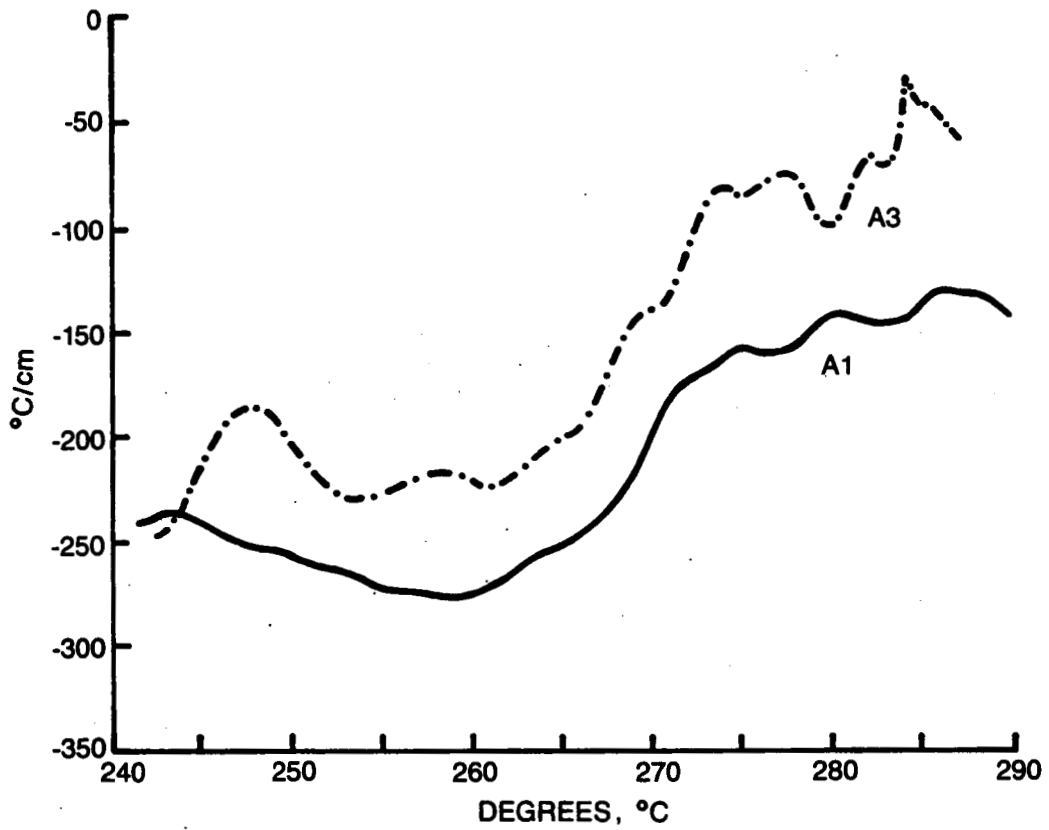
R87-3211-012G  
R87-3246-022G

A plot of thermal gradient versus sample temperature is shown in Fig. 9a and 9b for samples A1 through A4. Solidification in these plots progresses from right (temperature gradient in the melt) to left (temperature gradient in the solid). The region between these two gradient plateaus is the solidification zone. It is difficult to specify a solidification temperature for these samples since the solidification zone is rather wide (260 °C-270 °C). The small oscillations in temperature gradient can be attributed to unsteady furnace motion (Ref 19). There is no morphological evidence however, that the oscillations observed in the thermal data affected the growth of the samples: no banding could be detected in longitudinal cross-sections of these samples and microstructural changes were within experimental error. Note that in the thermal gradient curves samples A3 and A4, grown with the imposed magnetic field, show reduced thermal gradients over samples A1 and A2 which were grown without an applied magnetic field. That this is evidence of mixing is not clear since it also occurred in the Mn-rich samples whose macrosegregation results indicated reduced mixing. Thus, results appear somewhat inconclusive. However, an important difference is seen in the samples grown from a melt of 600 °C.

Samples A6 and A7 were grown with very high thermal gradients and morphological examination of longitudinal cross-sections of these samples showed significant differences in transitioning from dendritic to cooperative growth. As seen in Fig. 10, the transition region in sample A7 grown with an imposed 3 kG transverse magnetic field shows larger disturbances in rod orientation compared with that of A6 ( $B = 0$  kG).

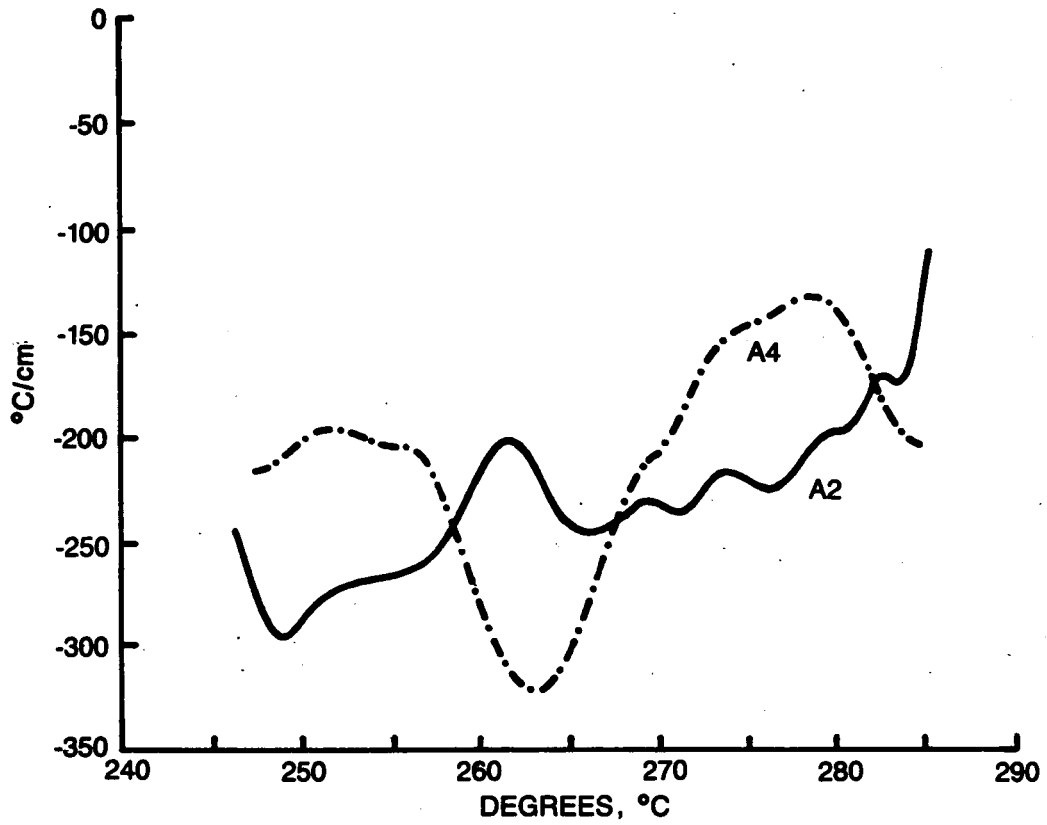
### 3.1.2 Composition B (0.52 w/o) Mn

Thermal gradient vs temperature curves for these samples are shown in Fig. 11. In comparison to composition A, the results of composition B showed a cleaner transition from melt to solid. Although melt temperatures were chosen at 450 °C for all cases, the thermal gradients again differed considerably between the samples grown with and without an applied 3 kG transverse magnetic field. In these samples, however, the composition profiles show significant macrosegregation differences for samples B1 through B4 shown in Fig. 12a and 12b. If we analyze the macrosegregation curves using stagnant film analysis as in Burton et al (Ref 20), a quantitative description



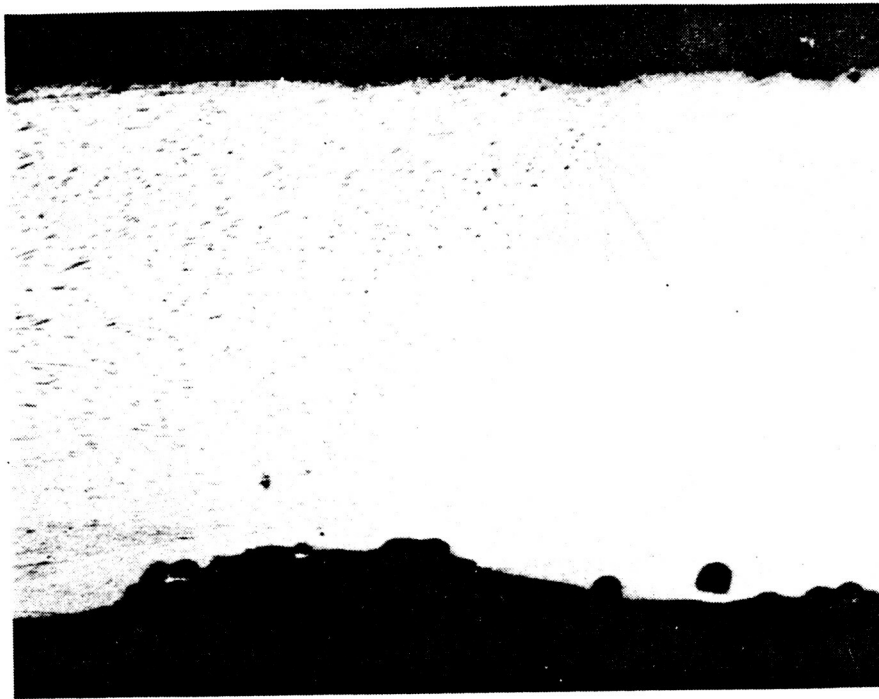
R87-3246-007G

Fig. 9a Temperature Gradient in Samples of Composition 0.2 w/o Mn Grown Up; A1 with an Applied Transverse Magnetic Field of B=0 kG and A3 with B=3 kG



R87-3246-008G

**Fig. 9b** Temperature Gradient in Samples of Composition 0.2 w/o Mn Grown Down; A2 with an Applied Transverse Magnetic Field of  $B=0$  kG, and A4 with  $B=3$  kG



Sample A6;  $B = 0$  kG

1 mm

←  
Growth  
Direction



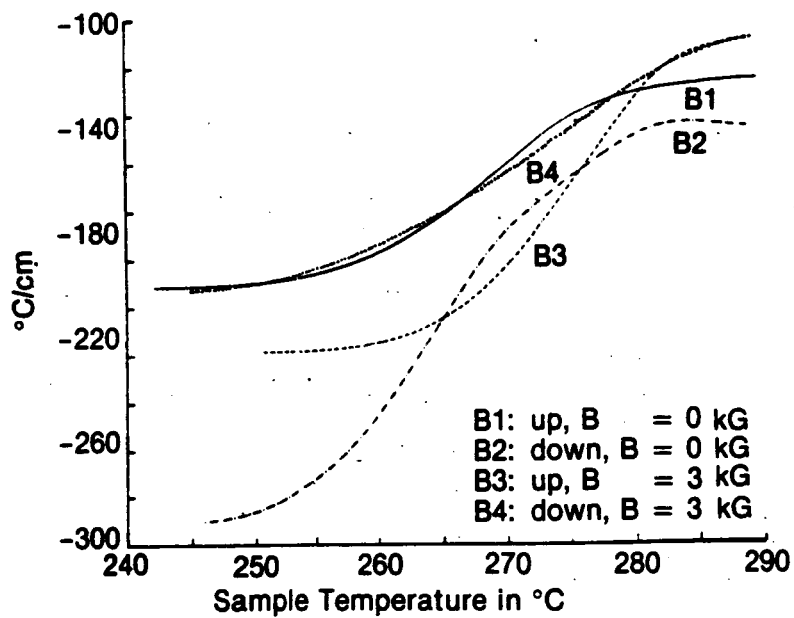
Sample A7;  $B = 3$  kG

1 mm

←  
Growth  
Direction

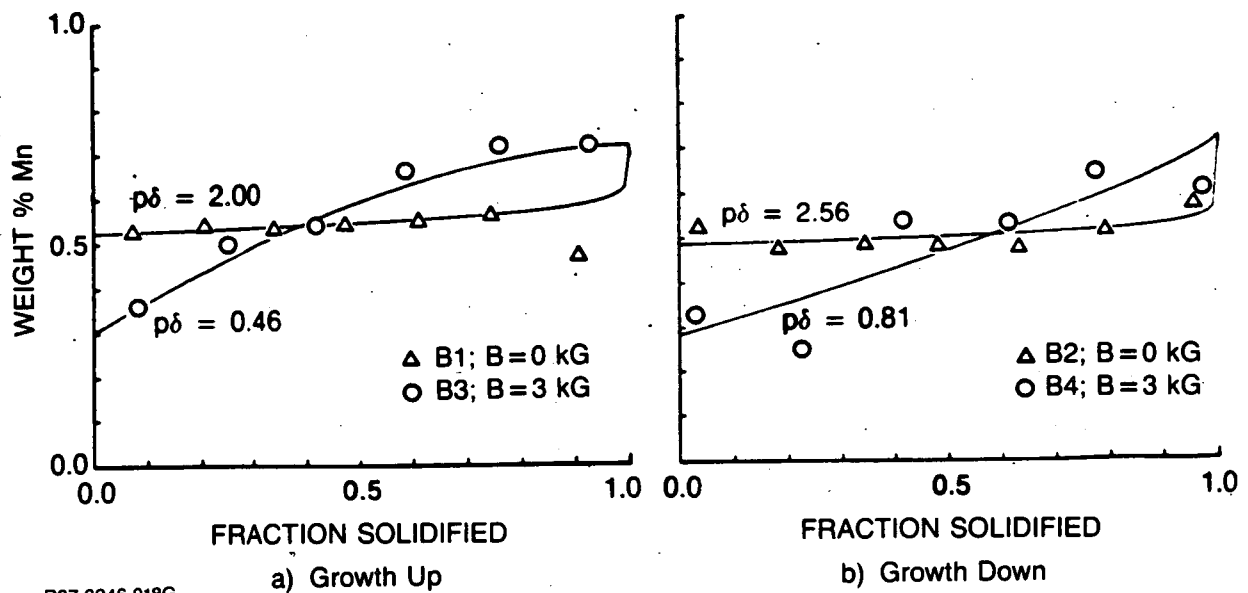
R87-3246-019G  
R87-3211-004G

Fig. 10 Comparison of Dendritic-cooperative Transition Regions of High Thermal Gradient Samples A6 and A7 Grown Up, with and without an Applied Transverse Magnetic Field. Melt Temperature was  $600^{\circ}\text{C}$ .



R87-3246-014G  
R87-3211-005G

**Fig. 11 Temperature Gradient in Samples of Composition 0.52 w/o Mn Grown Vertically Up and Down with and without an Applied Transverse Magnetic Field**



R87-3246-018G

Fig. 12 Longitudinal Composition Profiles for 0.52 w/o Mn Samples  
(with and without an Applied Transverse Magnetic Field)

of the macrosegregation can be obtained for off-eutectic growth using the formulation of Verhoeven et al (Ref 21). In this model, the average solid composition,  $\bar{C}_s$ , is described as a function of fraction solidified,  $f$ , for a closed system:

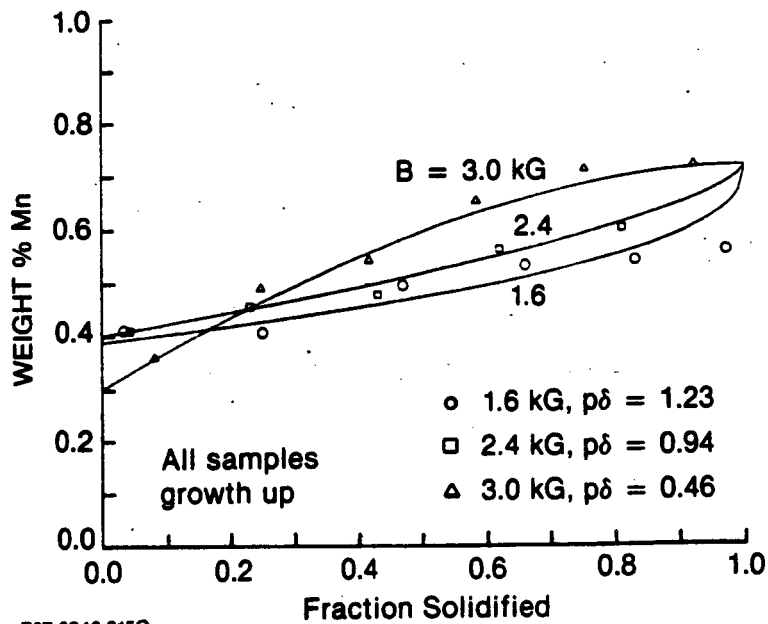
$$\bar{C}_s = C_C - \frac{(C_E - C_0)}{1 - e^{-p\delta}} (1-f)^{-1/(1-e^{p\delta})} \quad (5)$$

where  $p\delta = \delta/(D_L/V)$  and  $D_L$  = liquid diffusivity (assumed to be  $2 \times 10^{-5}$  cm<sup>2</sup>/s for the Bi-Mn compositions of interest and  $V$  = growth rate.  $\delta$  is the defined stagnant film length inside of which transport is assumed to be diffusion controlled. Fitting this equation to the test results using a graphical solution for  $p\delta$ , a higher degree of convection, lower  $p\delta$ , was observed for samples grown both up and down with the 3 kG transverse applied magnetic field than without an applied field. Quantitative morphological analysis of rod diameter on selected samples (Table 2) shows differences but these are within experimental errors. A clear demonstration of the effect of the imposed transverse magnetic field on mixing is demonstrated in Fig. 13 which shows macrosegregation curves for B samples grown upward in different applied magnetic fields. As the field strength decreases, a corresponding increase in  $p\delta$  is observed (cf., Table 1), indicating reduced mixing.

### 3.2 Mn-RICH SAMPLES

#### 3.2.1 Composition D (0.86 w/o Mn)

Samples in this group had a significantly different reaction to the imposed transverse magnetic field than the Bi-rich case. For Mn-rich growth, one would expect MnBi dendrites to solidify first, the sample transitioning to two-phase cooperative growth as  $C_L$  (solute concentration in the melt) approaches the eutectic. Instead, in the growth up orientation of the Mn-rich cases, MnBi dendrites grew and apparently separated from the interface freezing in the middle to top part of the sample. Previous studies (Ref 22 and 23) have not observed the effect of dendrite separation and floating. Dendrite separation can possibly be attributed to unsteady furnace motion. A sudden decrease in furnace motion can cause meltback of the interface (Ref 24) that may result in separation of the MnBi dendrites from their solidified positions. For growth parallel to gravity (downward), however, the MnBi dendrites were pinned at the interface and growth proceeded as expected.



R87-3246-015G  
R87-3211-007G

Fig. 13 Longitudinal Composition Profiles for 0.52 w/o Mn Samples Showing Variation Obtained in Macrosegregation with Different Applied Magnetic Field Strengths

Thermal results for all composition D samples showed, as in previous samples, suppressed thermal gradients as a result of the transverse magnetic field (Fig. 14). The growth down macrosegregation curves in Fig. 15 show that sample D4 (cf., Table 3), grown with the applied transverse magnetic field, had a higher  $p\delta$  than sample D2 (no magnetic field; 0.77 vs 0.36) and, therefore, lower mixing, in contrast to the results obtained with the Bi-rich composition B samples.

Table 4 compares the morphology of selected regions for composition D samples. Differences in rod diameter and interrod spacing generally fell within experimental error excepting the interrod spacing of sample D4 (down, B = 3 kG) which displayed reduction over D2 (down, B = 0 kG) indicative of decreased convection (Ref 15) and in agreement with the macrosegregation results for these two samples.

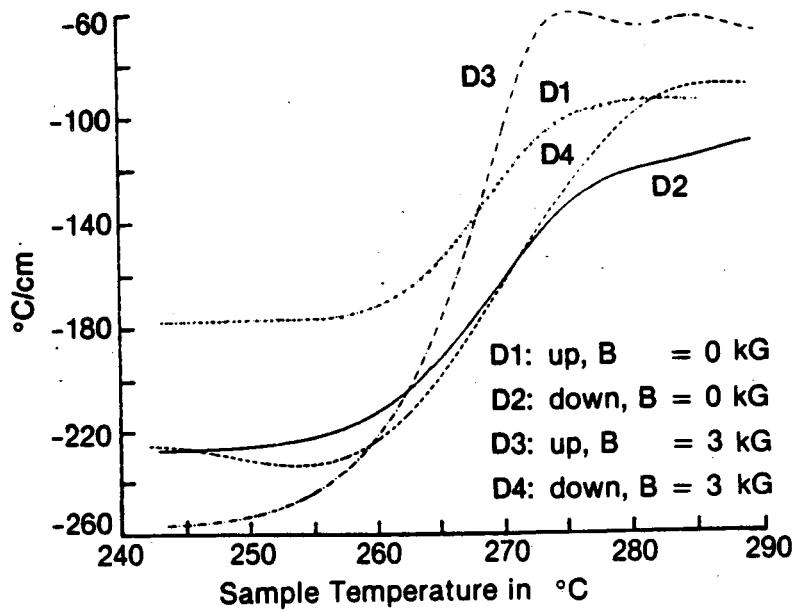
Although the thermal data in Fig. 14 exhibited a decreased thermal gradient for D4 over D2, no change in undercooling could be detected in the data as in the case of the Bi-rich (0.52 w/o Mn) samples where a shift towards reduced undercooling (increased convection) is observed (Fig. 8) with application of the 3 kG magnetic field. The interrod spacing results for D4 indicate, on the contrary, an increase in undercooling (decreased convection) if we apply a Hunt-Jackson type model (Ref 25) for rod eutectic growth relating interface undercooling,  $\Delta T$ , to mean growth velocity,  $V$ , and interrod spacing by

$$\Delta T = AV\lambda + B/\lambda \quad (6)$$

which indicates that a decrease in interrod spacing occurs with an increase in undercooling.

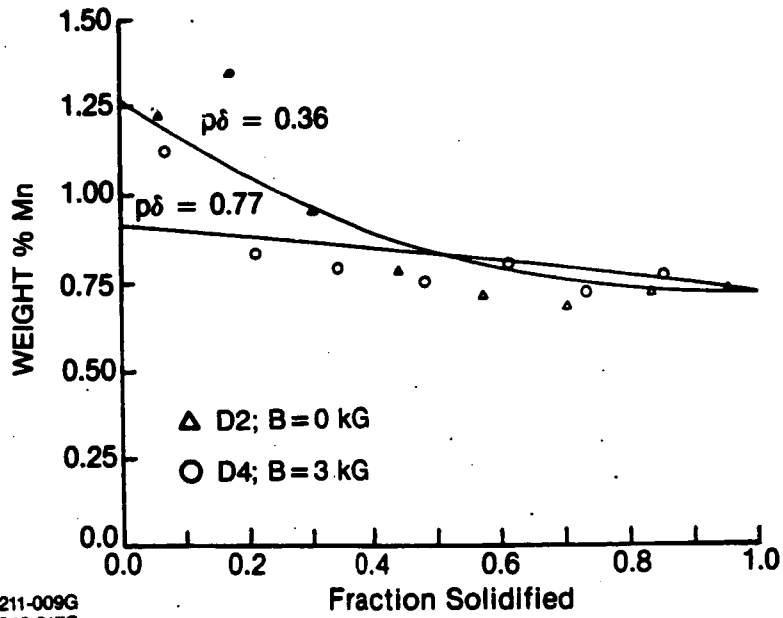
### 3.2.2 Composition E (1.5 w/o Mn)

Table 2 shows solidification data for composition E samples. Samples E1 and E3 displayed similar behavior to composition D samples (growth up) where MnBi dendrites separated from the interface and froze into the upper part of the sample. The macrosegregation curve for E1, shown in Fig. 16a, supports this. In E3 (up, B = 3 kG), however, even though a morphological examination of longitudinal cross-sectioning and the macrosegregation data, shown in Fig. 16b,



R87-3246-016G  
R87-3211-008G

**Fig. 14 Temperature Gradient in Samples of Composition 0.86 w/o Mn Growth Up and Down with and without an Applied Transverse Magnetic Field**



R87-3211-009G  
R87-3246-017G

Fig. 15 Longitudinal Composition Profiles for 0.86 w/o Mn Samples Growth Down with and without an Applied Transverse Magnetic Field

**Table 3 Solidification Characteristics of Mn-rich Samples**

<u>Sample</u>	<u>w/o Mn</u>	<u>Growth Rate (cm/h)</u>	<u>Growth Direction</u>	<u>Field Strength (kG)</u>	<u>G/V (°C-s/cm<sup>2</sup>)</u>	<u>pδ</u>
D1	0.92	10.9	up	0	$3.3 \times 10^4$	—
D2	0.89	10.4	down	0	$2.3 \times 10^4$	0.36
D3	0.78	10(est.)	up	3	$2.3 \times 10^4$ (est.)	—
D4	0.83	10(est.)	down	3	$3.2 \times 10^4$ (est.)	0.77
E1	1.46	0.78	up	0	$7.4 \times 10^5$	—
E3	1.38	0.7	up	3	$8.2 \times 10^5$ (est.)	—

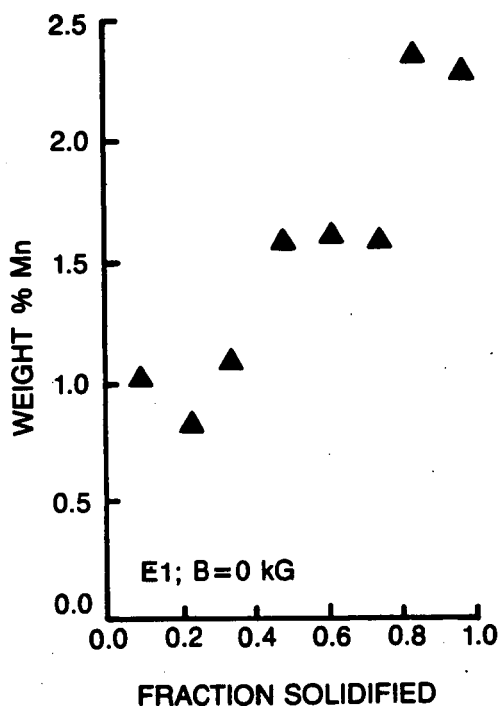
R87-3211-013G  
R87-3248-023

**Table 4 MnBi Mean Rod Diameters and Interrod Spacings for Selected Samples of Composition 0.86 w/o Mn**

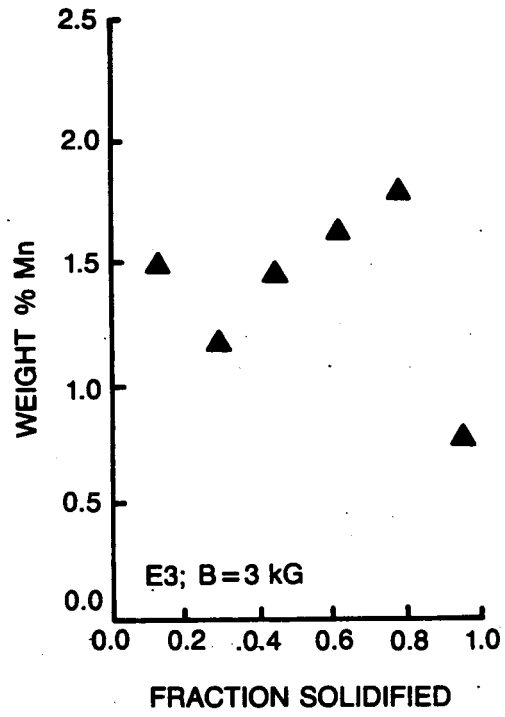
<u>Sample</u>	<u>D1e*</u>	<u>D2d</u>	<u>D3d</u>	<u>D4d</u>
Fraction solidified	0.80	0.45	0.50	0.48
Mean rod diameter	$0.458 \pm 0.156$	$0.786 \pm 0.216$	$0.607 \pm 0.178$	$0.643 \pm 0.183$
Mean interrod spacing	$1.853 \pm 0.65$	$3.48 \pm 1.13$	$2.52 \pm 0.79$	$2.52 \pm 0.83$
Growth	Up, B=0 kG	Down, B=0 kG	Up, B=3 kG	Down, B=3 kG

\*Sample had many dendrites present – not included in statistics

R87-3211-014G  
R87-3246-024G



(a)



(b)

R87-3246-009G

Fig. 16 Longitudinal Composition Profiles for 1.5 w/o Mn Samples Growth Up with and without an Applied Transverse Magnetic Field.

shows a higher concentration of dendrites in the upper part of the sample (bouyancy effect), there is significantly more uniformity in distribution of dendrites in E3 than in E1 ( $B = 0$  kG). Furthermore, the dendrites in E3 showed more uniform alignment (see Fig. 17).

### 3.3 High-field Eutectic Growth

The ADSF GE furnace was modified to fit the core of the 10L magnet at the Francis Bitter National Magnet Laboratory. An important feature of the furnace is that with the melt at  $450^{\circ}\text{C}$ , the external walls are only slightly above room temperature. This insures that no damage occurs to the magnet due to overheating.

A theoretical study of Bridgman-Stockbarger solidification in longitudinal magnetic fields (Ref 26) indicated that extreme high fields can cause mass transport at the melt-solid interface to become highly non-uniform and that specific growth conditions and material would determine an optimum field at which mass transport would be nearly uniform across the interface. As an initial look at this problem, one eutectic sample of Bi/MnBi (sample C1) was solidified using the conditions specified in the experimental section. In a preliminary analysis of the resulting growth, a longitudinal cross-section of the sample revealed that the 1 cm/h velocity appeared relatively unaffected by the magnetic field sweep from 0-40 kG. The 0.5 cm/h region (first half of the sample) had a reaction at the 16-18 kG level. Normal 1-g growth at 0.5 cm/h results in MnBi platelet growth (Ref 27) with random orientations. At these fields, however, there was clear rod eutectic growth (see Fig. 18), whereas other field values produced no discernible MnBi growth. Indicated for further study of this sample is transverse cross-sectional examination of rod diameter and interrod spacing per field value for the 1 cm/h region.

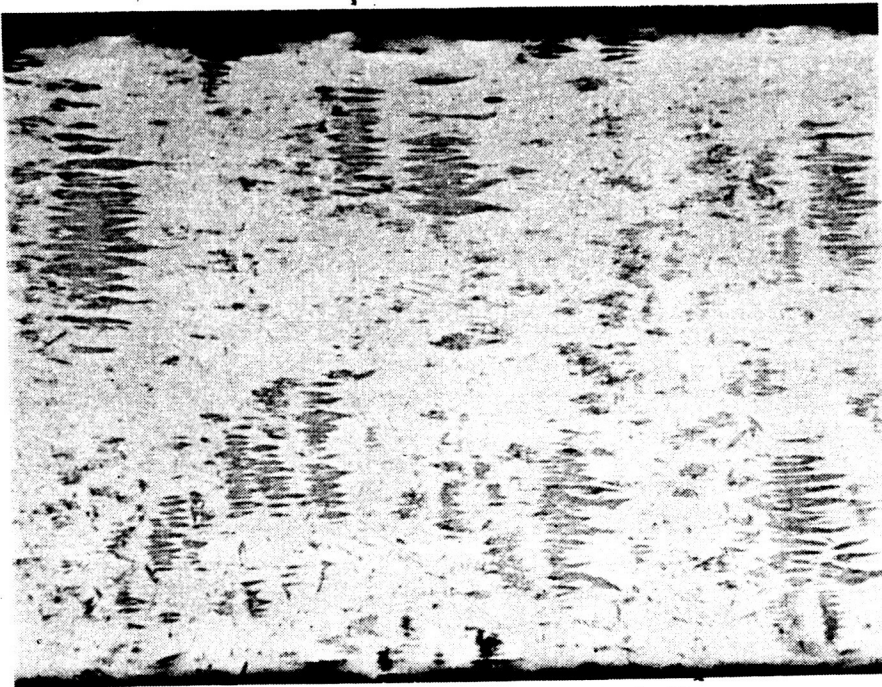
ORIGINAL PAGE IS  
OF POOR QUALITY

1 mm



Growth  
Direction

Sample E1; B = 0 kG



1 mm



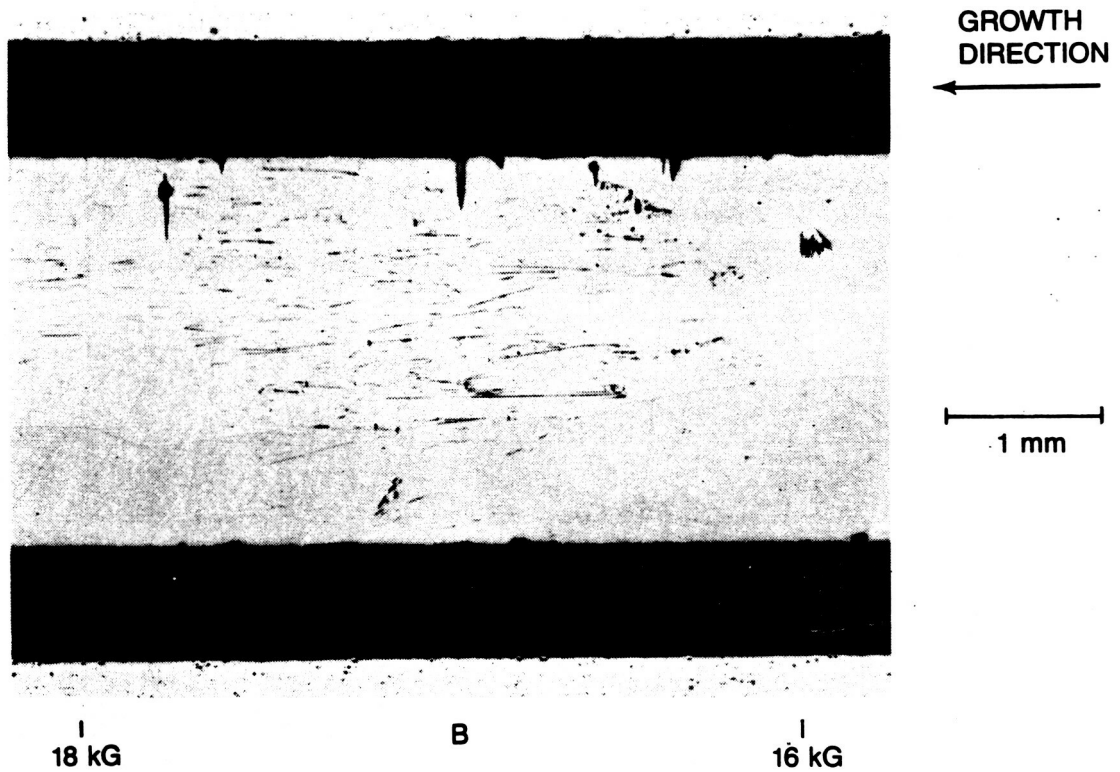
Growth  
Direction

Sample E3; B = 3 kG

R87-3246-020G  
R87-3211-010G

Fig. 17 Comparison of Dendrite Growth Behavior on Samples of 1.5 w/o Mn Growth Up, with and without an Applied Transverse Magnetic Field (Longitudinal Polish)

ORIGINAL PAGE IS  
OF POOR QUALITY



R87-3246-010G

**Fig. 18** Photomicrograph Showing Region of MnBi Rod Growth in a Eutectic Sample of Bi-Mn Grown Up at a Velocity of 0.5 cm/h in an Applied Longitudinal Magnetic Field Swept from 0 to 40 kG in 100 min

#### 4. SUMMARY Bi-Mn STUDY

The Bi-rich samples (compositions A and B) samples showed clear indications of increased mixing due to the application of a transverse magnetic field, irrespective of growth direction. The Mn-rich melts exhibited the inverse trend, where the transverse magnetic field appeared to inhibit convection resulting in samples with greater uniformity of solute distribution, although the data sampling was somewhat limited. The parameter of the solidification process that is responsible for this interaction with the transverse applied magnetic field may be fluid flow phenomena, conductivity anisotropies or a combination of both. It has been observed (Ref 28 and 29) that Mn in an alloy melt contributes one electron per atom towards liquid conductivities. In these studies, it was also found that in liquid alloys of Mn-Te, Mn-Sn, Mn-In and Mn-Sb, increased concentrations of Mn decreased conductivity of the liquid. By comparison it has been determined that Bi has an effective liquid conductivity of five electrons per atom (Ref 30). Moreover, one might anticipate similar liquid conductivity behavior in Bi-Mn alloys as has been observed in Mn-Sb, i.e., Bi-rich melts would be more conductive. Since the Lorentz force is directly proportional to the conductivity in the melt (Eq 1), conductive anisotropies (viz., Bi or Mn enriched solute at the interface due to solute rejection) may be quite significant.

The capability for directional solidification of Bi-Mn in high longitudinal magnetic fields has been established. A eutectic sample of Bi-Mn grown up at 0.5 cm/h in a magnetic field swept from 0 to 40 kG in 100 min. showed, in longitudinal cross-section, aligned rod growth at field values of 16-18 kG. Growth at 1 cm/h of eutectic Bi-Mn under the same conditions showed no evidence of the magnetic field affecting growth behavior from examination by longitudinal cross-sectioning.

PRECEDING PAGE BLANK NOT FILMED

5. PROGRAM ASSOCIATED PUBLICATIONS & PRESENTATIONS

1. DeCarlo, J., Pirich, R., and Dressler, B., "Effect of External Magnetic Fields on Directional Solidification of Bi-Mn Alloys," Francis Bitter National Magnet Laboratory Annual Report, Cambridge, MA, 1985.
2. DeCarlo, J., and Pirich, R., "Effects of an Applied Magnetic Field on Directional Solidification of Off-Eutectic Bi-Mn Alloys," presented at the MRS Fall Mtg, Boston, MA, Dec 1-5, 1986.

PRECEDING PAGE BLANK NOT FILMED

## 6. ACKNOWLEDGMENTS

The authors wish to express their appreciation to B. Dressler and W. Poit for their experimental work on the program and also to Drs. D. Larson, J. Bethin, and M. Glicksman for their many helpful discussions. We would also like to thank Drs. R. DeIasi and P. Adler for their technical guidance and encouragement, and especially B. Brandt and L. Rubin of the Francis Bitter National Magnet Laboratory for their technical assistance and suggestions.

PRECEDING PAGE BLANK NOT FILMED

## 7. REFERENCES

1. Flemings, M., Solidification Processing, New York: McGraw-Hill, 1974.
2. Pirich, R., Larson, Jr., D., and Busch, G., IEEE Trans., Vol MAG-15, No. 6, 1979, p 1754.
3. Pirich, R., IEEE Trans., Vol MAG-16, No. 5, 1980, p 1065.
4. Boettinger, W., Biancaniello, F., and Coriell, S., Met. Trans A, Vol 12A, 1981, p 321.
5. Pirich, R., Larson, D., and Busch, G., AIAA J., Vol 19, 1981, p 589.
6. Gatos, H., Materials Processing in the Reduced Gravity Environment of Space, Rindone, G., ed., New York: Elsevier Science Publishing Co., 1982, p 355.
7. Pirich, R., and Larson, D., Grumman Research Department Report RE-602, 1980.
8. Pirich, R., Grumman Research and Development Center Report RE-642, 1982.
9. Bethin, J., Grumman Research and Development Center Report RE-691, 1984.
10. Utech, H., and Flemings, M., Crystal Growth, New York: Pergamon Press, 1967, p 651.
11. Kim, K., J. Electrochem Soc., Vol 129, No. 2, 1982, p 427.
12. Witt, A., Herman, C., and Gatos, H., J. Mater. Sci., Vol 5, 1970, p 822.
13. DeCarlo, J., and Pirich, R., Grumman Research and Development Center Report RE-680, 1984.
14. DeCarlo, J., and Pirich, R., Met. Trans A, Vol 15A, 1984, pp 2155-2166.
15. Baskaran, V., Eisa, G., and Wilcox, W., Computational Methods and Experimental Measurements, Proc. of the 2nd Int. Conf., QE2, NY to Southampton, 1984, pp 219-230.
16. Mollard, F., and Flemings, M., Trans AIME, Vol 239, 1967, p 1526.
17. Tiller, W., Jackson, K., Rutter, J., and Chalmers, B., Acta Metallurgica, Vol 1, 1953, p 428.
18. Buscemi, C., Grumman Corporate Research Center, Bethpage, NY, Unpublished research, 1982.
19. DeCarlo, J., Grumman Corporate Research Center, Bethpage, NY, Unpublished research, 1985.

PRECEDING PAGE BLANK NOT FILMED

20. Burton, J., Prim, R., and Slichter, W., J. Chem. Phy., Vol 21, No. 11, 1953, p 1987.
21. Verhoeven, J., and Homer, R., Met. Trans., Vol 1, 1970, p 3437.
22. Pirich, R., Larson, D., Wilcox, W., Fu, T., Ravishankar, P., Remarao, B., Nair, M., and Doddi, K., Grumman Research and Development Center Report RE-649, Jan 1983.
23. Pirich, R., Materials Processing in the Reduced Gravity Environment of Space, Rindone, F., ed., New York: Elsevier Science Publishing Co., 1982, p 593.
24. Fu, T., and Wilcox, W., J. Crys. Growth, Vol 51, 1981, p 557.
25. Jackson, K., and Hunt, J., Trans AIME, Vol 236, 1966, p 1129.
26. Oreper, G., and Szekely, J., J. Crystal Growth, Vol 67, 1984, pp 405-419.
27. Pirich, R., Met. Trans A., Vol 15A, 1984, p 2162.
28. Okada, T., and Ohno, S., J. Phys. Soc. Japan, Vol 55, No. 2, 1986, p 599.
29. Gasser, J., and Kleim, R., Liquid Metals 1976, Evans and Greenwood, eds., London: The Institute of Physics, 1977, p 352.
30. Mott, N., and Jones, H., The Theory of the Properties of Metals and Alloys, New York: Dover, 1958.